nature climate change

ARTICLES

https://doi.org/10.1038/s41558-019-0454-4

Advances in phenology are conserved across scale in present and future climates

David N. Laskin[1]*, Gregory J. McDermid[1], Scott E. Nielsen[2], Shawn J. Marshall[1], David R. Roberts[1] and Alessandro Montaghi[1]

Warming temperatures are advancing the timing of seasonal vegetation development in the extratropics, altering plant–animal interactions and increasing the risk of trophic asynchrony. Forest understories are critical yet under-observed ecosystems in which phenological patterns are both altered and obscured by overstory trees. We address the challenge of observing phenological dynamics in the understory by exploiting the physiological relationship between plant phenology and temperature accumulation, a horticultural principle we show to be preserved across spatial scales through a combination of field and growth-chamber observations. These observations provide the foundation for a spaceborne thermal-observation framework, which can trace the discrete phenophases of forest understory plants in near-real time. The thermal basis of this framework also enables the prediction of understory phenology for future climates, which we demonstrate here using *Shepherdia canadensis*, a widespread fruiting shrub of western North America that has important trophic connections to frugivores. Our approach enables researchers to assess the regional-scale impacts of climate change on bottom-up forest ecosystems and to monitor emerging trophic mismatches.

In the extratropics, climate is the main factor controlling rates of plant development, owing to the plants' intrinsic reliance on temperature[1]. As a result, changes in vegetation phenology have been one of the first-observed effects of climate change[2], with warming temperatures advancing reproductive development of vegetation[3]. This results in temporal shifts of bottom-up ecosystem processes such as the alteration of habitat-use strategies of plant-dependent fauna[4], and can trigger the complete decoupling of trophic interactions[5]. In addition to being an indicator of climate change, phenology provides fundamental insights into ecosystem function across scales, from individuals to landscapes[6,7]. However, there is no detailed knowledge of how future climate change will affect the scale and interaction of phenological processes[8]. An observation framework is needed that can accurately capture phenological dynamics in both space and time.

Time-series analyses of remote-sensing imagery in the optical wavelengths now routinely deliver land-surface phenology metrics on a global scale[9], including observations of spring onset, autumn senescence and seasonal maxima[10]. However, these metrics are typically inferred from spectral indices that integrate the overall 'greenness' of an image pixel, and are generally too coarse to be linked to discrete, species-specific phenophases such as fruiting[11]. These limitations are further exacerbated in forests, where overstory canopies both influence the development of plants in the understory and mask them from detection by spaceborne instruments. Considering that forests harbour two-thirds of Earth's terrestrial biodiversity[12], De Frenne and Verheyen[13] recently stressed the importance of focusing global attention to the lack of microclimate analyses beneath the canopy.

We used growing degree days (GDDs), the well-known horticultural principle linking plant development to thermal units of temperature accumulation, as an instrument for observing forest understory phenology. Using satellite-derived estimates of understory temperature (T_{ust}), we developed a monitoring framework that generates reliable daily maps of species-specific phenophase progression in near-real time. Here, we demonstrate this framework using the Canada buffaloberry (*Shepherdia canadensis*), a fruiting perennial shrub that is widespread in western North America. In addition to enabling contemporary monitoring of forest understory species, the mechanistic, thermal foundation of our framework also enables us to predict the phenological response of understory plants under future climate scenarios. As an example, we examine how *S. canadensis* phenology might respond to an end-of-century warming of +3.3 °C in our study region, on the basis of the IPCC Fifth Assessment Report (AR5) representative concentration pathway (RCP) 4.5.

Tracking phenology from plants to landscapes

The reliability of using temperature accumulations as a common reference for phenological development in plants is long established[14]. This consistency is largely due to the principle that the amount of heat required to advance from one life cycle stage to the next generally does not change[15]. Thermal time is often expressed in GDDs, which are much better for predicting phenological events than other approaches such as time-of-year or number-of-days[16]. Plants have unique minimum base temperatures below which physiological development does not occur. Once this threshold is determined, it is possible to establish a reference point to commence GDD accumulations (AGDD)[17]. When the threshold has been surpassed, rates of development increase approximately linearly as a function of air temperature[18].

We assessed the spatiotemporal variability of reproductive development of *S. canadensis*. This fruiting dioecious shrub is common throughout the southern Rocky Mountains of Canada, and provides critical nutrition for a wide variety of foraging species. Accordingly, our 125,000 km^2 study area was established on the range extent of a threatened population of grizzly bears (*Ursus arctos*), for which *S. canadensis* is an essential food source[19] (Fig. 1). Phenology

[1]Department of Geography, University of Calgary, Calgary, Alberta, Canada. [2]Department of Renewable Resources, University of Alberta, Edmonton, Alberta, Canada. *e-mail: dnlaskin@ucalgary.ca

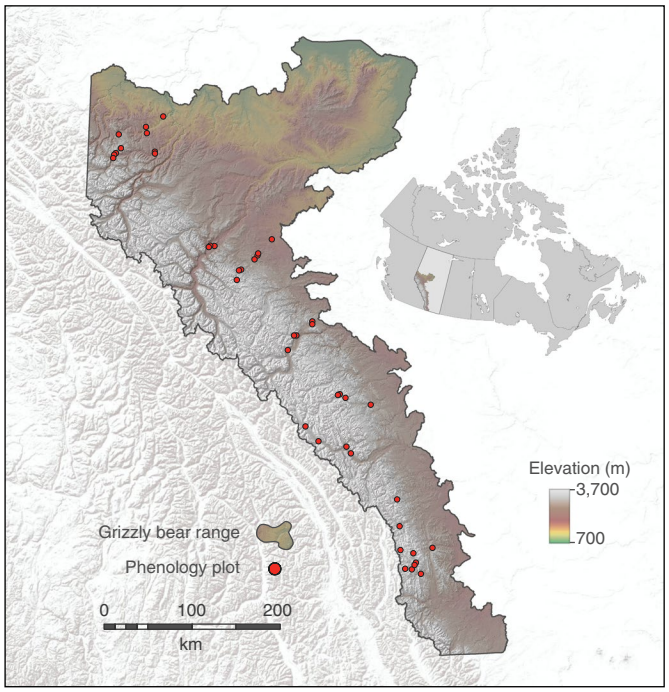

Fig. 1 | The extent of the study area in the Rocky Mountains of western Alberta, Canada. The study area encompasses the entirety of the grizzly bear (*U. arctos*) range in the province. Forty-five understory phenology observation plots were distributed throughout a variety of forest types and elevation profiles.

observations were made with time-lapse cameras in 45 forested plots and corroborated by regular field visits[20]. Twenty-nine of these plots were 250 m × 250 m (6.25 ha), in an attempt to unify observation scales on the ground with the Moderate Resolution Imaging Spectroradiometer (MODIS) satellite imagery[21].

We derived the AGDD requisite for each phenophase using the developmental stages identified in the in situ time-lapse imagery and associated T_{ust} field measurements. AGDDs were established on a developmental base temperature (t_b) that we estimated to be 0 °C ± 0.6 °C (t_b = 0 °C)[22]. Landscape-scale phenology maps were created for the following year by summing the thermal requirements in each pixel of a daily average T_{ust} image stack (Fig. 2). This daily T_{ust} imagery was derived from land-surface temperature (LST) measurements collected by the MODIS sensor overhead. The maps successfully predicted the complete incremental progression of reproductive phenology of *S. canadensis* in 16 validation locations. There was no significant difference between observations of phenophase timing in the landscape-scale maps and observations of individual plants on the ground (t = −0.08; P = 0.937; correlation coefficient = 0.986). The occurrence of fully ripe fruit was accurately predicted with a mean absolute error (MAE) of ±2.4 d on the individual plants (Fig. 3a). Of the 12 reproductive phenophases, the average start dates of the first 10 were estimated across the study area to an average of 1.4 d and the final two senescing phenophases at 3.3 d (Fig. 3b). In general, the maps have a very slight bias to underpredict development preceding fruit emergence, and to overpredict the timing of fruit maturation. For example, the average date of full-fruit maturation observed in situ was 31 July 2012, whereas the maps estimated this date to be 1 August 2012.

T_{ust} can be predicted from satellite despite trees and clouds

Our phenology mapping framework differs from existing approaches in that it uses thermal imagery to track the temperature-accumulation patterns of specific plant species in forest understories. We derived T_{ust} maps to discern fine microclimatic characteristics that are not available from interpolated weather-station data[23]. The MODIS sensor does not measure air temperature directly, but rather the skin temperature (emissivity) of the surfaces visible to the satellite in the form of LST[24]. Surface air temperature is then derived using a supplementary estimation technique[25]. However, microclimates within forests are out of view of the sensor, as canopies form relatively opaque boundaries between the understory and supra-canopy air masses. As a result, canopy-modified air temperatures in the understory drive phenological processes at different rates than those beyond the forest[26].

We were able to produce instantaneous spaceborne measures of T_{ust} (at time of satellite overpass) to within ±1.4 °C of in situ measurements (R^2 = 0.89) using empirical models that incorporate compositional and structural canopy metrics[27]. To provide a thermal basis for broad-scale phenology maps, these instantaneous T_{ust} plot-scale estimates were extended to make spatially continuous maps of daily average T_{ust}. Persistent cloud cover often created large spatial and temporal gaps in our observation records[28]. On average, only 23% of the plot overpasses occurred during clear-sky conditions (n = 4,153). A common solution to mitigate data loss is to aggregate daily LST imagery into 8-day and 16-day composites. However, these composite periods are often too temporally coarse to distinguish short-lived phenological events[29]. Capturing the sudden appearance of phenophases like fruit-ripening requires daily observations[30]. We use generalized linear models to estimate average daily T_{ust} from each of the four daily MODIS overpasses to within ±1.5 °C ($R^2 \approx 0.87$). By combining the cloud-free regions from each overpass, usable pixel coverage increased considerably[31]. Remaining cloud gaps were filled using a Gaussian-weighted temporal interpolation[32]. The final daily average T_{ust} images were enhanced to 250 m spatial resolution[33] and were accurate to ±2.2 °C in all weather conditions, including times of persistent cloud cover.

Predicting understory phenology in future climate scenarios

We used the same method of temperature accumulation to forecast the effects of climate warming by integrating a future thermal anomaly into the T_{ust} maps. The moderate end-of-century warming scenario RCP4.5 was downscaled to a 1-km resolution anomaly surface for the extent of the study area[34]. The regional anomaly averaged 3.3 °C (global likely range is 1.7–3.2 °C), and was added to the present-day T_{ust} image stack to produce projections of 2071–2100 phenology (hereafter referred to as 2080s). Warming is also expected to alter the distribution of plant habitat as plants exploit new niches made available by a changing climate[35]. Therefore, we produced habitat-distribution models for both the present day (1961–1990) and the 2080s to spatially mask the phenology maps. To assess phenological timing at the landscape level, we used peak coverage, based on the date when the maximum number of image pixels transition to the next phenophase. Parmesan[36] highlights the difficulty measuring phenology in a generalized way; average dates do not really work, hence peak coverage is deemed more ecologically contextual.

Our maps forecast a significant advance in all *S. canadensis* phenophases, including a 13-day shift in florescence and a 19-day advance in the development of fully ripe berries (Fig. 4). The rate of ripening increases with elevation; the subalpine regions of the study area are projected to experience a full 37-day shift. We predict the range of the *S. canadensis* habitat to decline by 8% (−4,510 km²)—a sizable decrease considering the time horizon (60 to 80 years). However, there will be an increase in ripe berries available during peak coverage (+4,150 km²). To control for modifiable areal unit problems and focus solely on the impact of warming, we also measured peak coverage at the present habitat extent (Fig. 5).

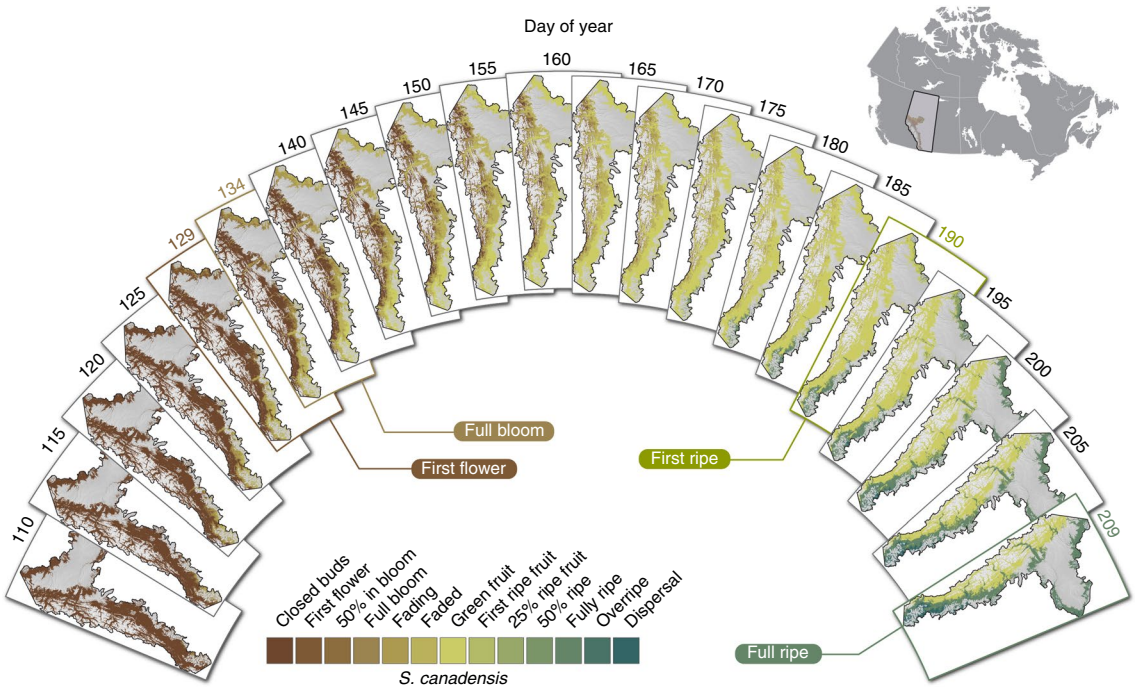

Fig. 2 | The complete sequential phenology of *S. canadensis*. The observation framework outputs a daily chronology of reproductive development for each discrete phenophase from closed bud to dispersal at 250-m resolution, shown here in 5-day increments for the present day (2012). The example highlighted phenophases indicate the timing of their peak spatial coverage within the study area.

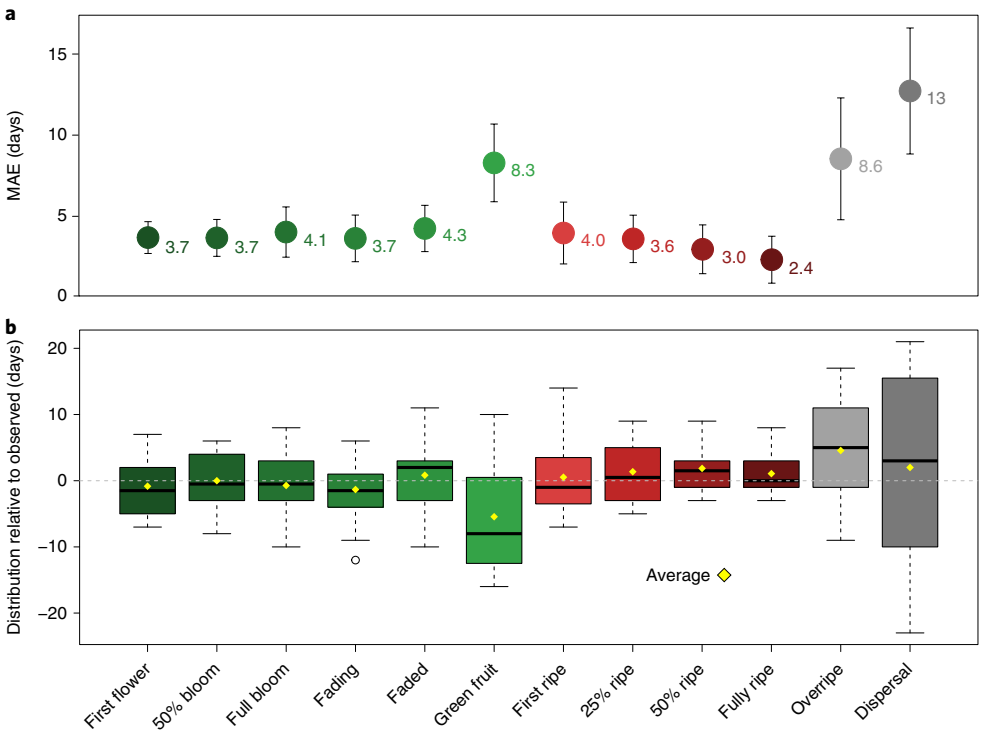

Fig. 3 | Variability in phenology map predictions of phenophase start dates for individual plants. a, The MAE of map predictions of phenophase start dates of individual plants observed in situ. Coloured points represent the error (in days) of the in situ observations (*x* axis) for each respective phenophase, with bootstrapped 95% confidence intervals. **b**, The distribution of start dates predicted by the phenology maps versus start dates observed in situ (dotted centre line shows in situ start dates). Diamonds indicate the observed study area average; box edges denote upper and lower quartiles; whiskers, maximum and minimum map estimates within 1.5× the interquartile range; outliers shown beyond whiskers; bold centre line indicates median map estimate.

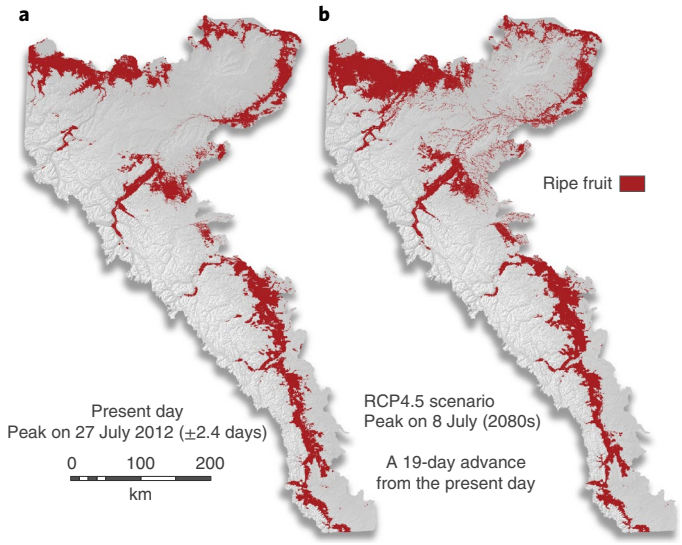

Fig. 4 | Shift in the peak spatial coverage of ripe fruit between the present day and the RCP4.5 scenario. a,**b**, Highlighted regions show the extent of peak spatial coverage of fully ripe fruit, which represents the height of available nutrition for frugivores at the landscape-scale for the present day (2012; **a**) and the forecast 2080s extent (**b**). Under the RCP4.5 scenario there is a predicted 19-day advance in the development of fully ripe fruit, accompanied by an 8% decline in *S. canadensis* habitat overall (−4,510 km^2). There is also a predicted increase of 4,150 km^2 in peak coverage during this same phenophase over the present day.

To evaluate our model predictions, we performed growth-chamber warming experiments to assess future phenological response at the scale of the individual plant. These experiments establish an observable temporal advance to compare with the hypothetical future phenology expressed in the maps. One bank of Conviron fully enclosed climate-controlled growth chambers was programmed to reflect present-day temperature within the study area (30-year normal); another bank was used to approximate the downscaled RCP4.5 warming scenario within our study area (mean +3.3 °C). After two seasonal observations, the plants under the warming scenario experienced an average of 12-day advance in florescence and a 35-day advance in ripening. These shifts are similar to those forecast in the mapped projections: 13 d for florescence and 37 d for ripening at high elevations (Fig. 6).

Discussion

Until now, the functionality of satellite-derived AGDD for monitoring understory phenology has been relatively unexplored. Our thermal-mapping framework was highly effective in pinpointing stages of understory plant development and demonstrates the strong, scale-invariant link between air temperature and plant physiology. Most land-surface phenology models infer developmental timing from a seasonal curve based on satellite-derived spectral indices (for example, ref. [10]). These curves work well for dealing with cloud-punctuated datasets and for detecting the pronounced spectral shifts associated with greenup and senescence. They are, however, less sensitive to discrete changes in mid-season phenology, especially beneath the forest canopy. The incorporation of thermal time (AGDD) in recent studies, including ours, is rapidly improving estimates of phenological timing. For example, Crimmins et al.[37] and Melaas et al.[38] used Daymet daily 1-km gridded meteorological surfaces to produce broad-scale estimates of spring leaf emergence and bloom to within 5 d for a number of forest species. However, the focus of these studies remains on spring onset, with the exception of Crimmins et al.[37], whose ripe-fruit estimates did not meet their model criteria of MAE ≤10 d. The Daymet temperature grids are interpolated from meteorological stations; this process inherently introduces spatial uncertainty as the distance between stations can be substantial[23]. Izquierdo-Verdiguier et al.[39] state that satellites overcome these interpolation issues, but meteorological station data are easier to relate to phenology observations on the ground—our approach appears to effectively bridge this gap.

The major assumption of our framework is that temperature controls the rate of phenological development in plants. This is largely true in regions with marked seasonal climates[40]. However, we found the thermal approach to be limited in estimating late-season phenophases. The timing of overripe berries and their dispersal is influenced by factors other than temperature, and is therefore difficult to predict with our approach. Whereas temperature will affect the rate at which berries desiccate, dispersal can occur from predation or simply a gust of wind. Predictions of late-season phenology could be improved by incorporating chilling degree days (CDDs). Yu et al.[41] found late-season CDDs to be an important predictor of leaf colouration and senescence, but many of the physiological controls of senescence remain ambiguous and are likely to extend beyond air temperature[11,42].

Our framework proved to be reliable despite the omission of other common attributes such as soil quality, available nutrients, photoperiod and humidity—which are all known to affect plant phenology. This simplicity is one of the main benefits of our approach, although further refinement with other factors is possible. For instance, Liang et al.[43] found that understory plant phenology could be strongly affected by day-to-day changes in humidity. Though we did find a significant difference in in situ plot humidity across the study area (2011: $F = 52.1$, $P < 0.01$; 2012: $F = 340.8$, $P < 0.01$), the practical variance in humidity ranged only between 3% and 10%. Although seemingly minor, these differences could affect rates of plant development. In future, site moisture derived from the MODIS thermal bands could be incorporated into the framework[44], particularly in future-scenario modelling, as most projections predict increased precipitation in the mid-latitudes[45].

Our observations provide a compelling, mechanistic strategy for exploring hypothetical future phenology patterns. With no way to truly validate future events, growth-chamber simulations worked in proxy to effectively test the sensitivity of *S. canadensis* to warming, operating on the same thermal foundation as the phenology maps. Although incorporating the RCP4.5 scenario resulted in marked shifts in the future phenology and distribution of *S. canadensis*, it is unlikely that these projected changes, over this timescale, would result in the collapse of trophic linkages on which these forest ecosystems depend. Nonetheless, such projections present concern regarding general trophic synchrony, which could consequently affect how frugivores use the landscape. For the grizzly bear, the apex omnivore in the study area, a nearly three-week projected advance in fruit ripening will produce a larger gap between the availability of this critical nutrition source and the time of hibernation. This would potentially lead to food deprivation as grizzly fecundity is highly linked to pre-hibernation body-fat percentage[46]. There is also a risk of phenological synchronization, where advancing availability of berries may begin to overlap with another preferred ephemeral nutrition source. For instance, grizzly bears in coastal Alaska are abandoning their role as critical nutrient dispersers in forest ecosystems as they are opting to eat berries over salmon owing to the recent harmonization of the phenologies of these two food sources[47].

There are many benefits to forecasting the impacts of climate change on phenology, but there are also advantages to looking to the past. Izquierdo-Verdiguier et al.[39] used Daymet and the cloud-computing capacity of Google Earth Engine to model 36 years of spring phenological indices over the conterminous United States. The temporal depth of this time series was able to resolve

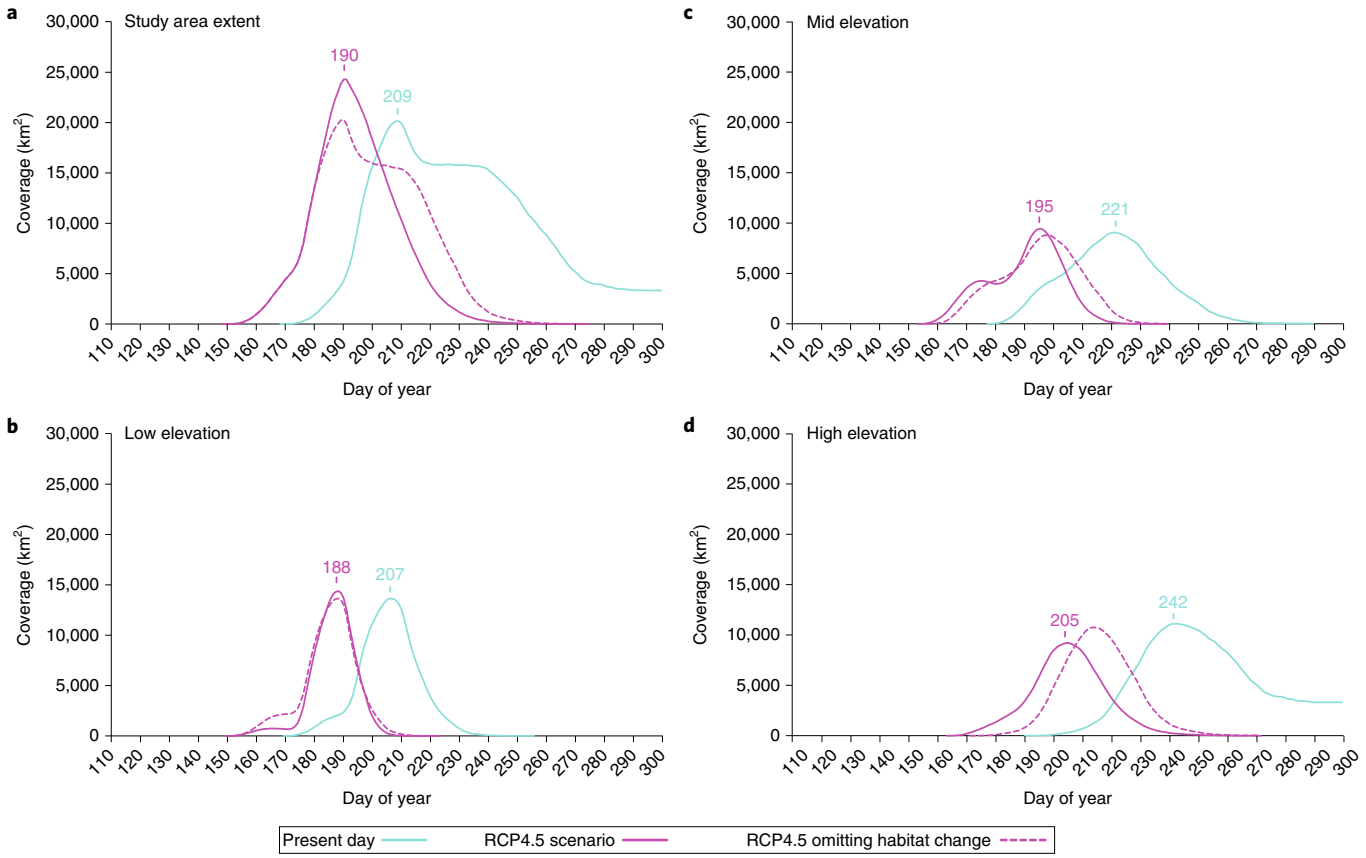

Fig. 5 | Seasonal spatial coverage of ripe fruit for the present day and the RCP4.5 warming scenario. Curves illustrate the area (in km²) of the landscape covered by fully ripe *S. canadensis* fruit throughout the growing season and the timing (day of year highlighted) of peak coverage for the present day and the RCP4.5 scenario assuming no change in the extent of *S. canadensis* habitat in the future (dotted line). **a**–**d**, The seasonal spatial coverage of ripe fruit across the study area (**a**), and for spatially equal tertile elevation ranges to exemplify differences in the regional effect of climate warming: low(<1,232 m; **b**), mid (1,233–1,561 m; **c**) and high (>1,562 m; **d**).

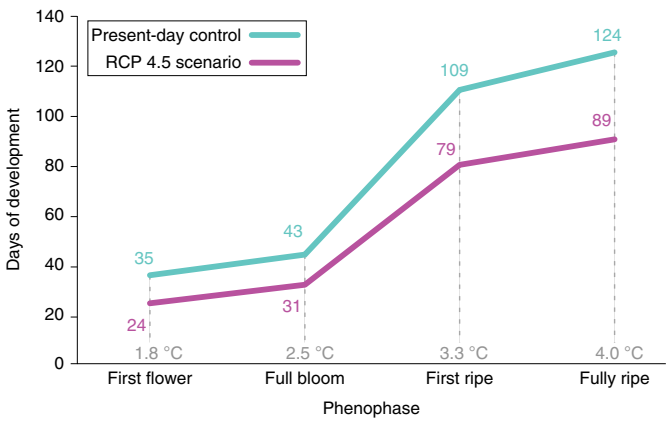

Fig. 6 | Difference in phenophase timing between the RCP4.5 (2080s) and present-day (1961–1990) growth-chamber scenarios. Experimental warming of *S. canadensis* ($n=46$) showing differences in combined observations of developmental phenophase timing between simulated present-day temperatures (1961–1990 normal) and the RCP4.5 warming scenario (downscaled regional anomaly). Temperature values indicate the difference in mean chamber temperatures preceding each phenophase.

long-term regional trends in spring onset, illustrating the potential for similar processing of the MODIS LST archive, albeit for only half this duration. Many recent studies have used the USA National Phenology Network (USA-NPN), which now has 15 million observation records for over 1,200 species with corresponding GDD requirements (for example, refs. [37–39]). Our framework is extensible to the USA-NPN and other global networks containing species with defined phenology, mainly in distinctly seasonal northern temperate, boreal and Arctic regions. For example, we tested this extensibility with a second species, *Hedysarum alpinum*, a perennial forb with a large taproot having a radically different developmental physiology to *S. canadensis*. As with the analysis presented here, we found no significant difference in the timing of predicted *H. alpinum* phenology and in situ observations ($t=-0.058$; $P=0.954$; correlation = 0.964). High-latitude climates are currently experiencing rates of warming two to three times the global average[48], and require reliable projections of plant community change critical to conservation and management in these areas.

Increasingly efficient access to MODIS LST imagery makes investigations into ecosystem phenology patterns and dynamics a timely benefit during a period of rapid environmental change[49]. Our remote-sensing approach can functionally examine trends in phenological changes in response to interannual seasonal differences as well as intra-season phenological progress to anticipate critical ecosystem events. The mapping framework provides near-real-time extensibility to choose any day of the season and determine the precise spatial extent of any phenophase, particularly with MODIS LST data often publicly available only a few days after acquisition[50]. Further, combining this methodology with high processing efficiency and extensive image archives, such as those within Google Earth Engine, will at once expand the global extensibility of this

framework. Maps are conventionally static and unchanging, but ecosystem processes are not.

Online content

Any methods, additional references, Nature Research reporting summaries, source data, statements of data availability and associated accession codes are available at https://doi.org/10.1038/s41558-019-0454-4.

Received: 25 March 2018; Accepted: 11 March 2019;
Published online: 15 April 2019

References

1. Reeves, P. H. & Coupland, G. Response of plant development to environment: control of flowering by day length and temperature. *Curr. Opin. Plant Biol.* **3**, 37–42 (2000).
2. Root, T. L. et al. Fingerprints of global warming on wild animals and plants. *Nature* **421**, 57–60 (2003).
3. Parmesan, C. Ecological and evolutionary responses to recent climate change. *Annu. Rev. Ecol. Evol. Syst.* **37**, 637–669 (2006).
4. Pearson, R. G. & Dawson, T. P. Predicting the impacts of climate change on the distribution of species: are bioclimate envelope models useful? *Glob. Ecol. Biogeogr.* **12**, 361–371 (2003).
5. Kerby, J. T., Wilmers, C. C. & Post, E. in *Trait-Mediated Indirect Interactions: Ecological and Evolutionary Perspectives* (eds Ohgushi, T. et al.) 508–525 (Cambridge Univ. Press, 2012).
6. Post, E. S. & Inouye, D. W. Phenology: response, driver, and integrator. *Ecology* **89**, 319–320 (2008).
7. Thackeray, S. J. et al. Phenological sensitivity to climate across taxa and trophic levels. *Nature* **535**, 241–294 (2016).
8. Garcia, R. A., Cabeza, M., Rahbek, C. & Araújo, M. B. Multiple dimensions of climate change and their implications for biodiversity. *Science* **344**, 1247579 (2014).
9. Buitenwerf, R., Rose, L. & Higgins, S. I. Three decades of multi-dimensional change in global leaf phenology. *Nat. Clim. Change* **5**, 364–368 (2015).
10. Zhang, X. Y. et al. Monitoring vegetation phenology using MODIS. *Remote Sens. Environ.* **84**, 471–475 (2003).
11. Nijland, W., Bolton, D. K., Coops, N. C. & Stenhouse, G. Imaging phenology: scaling from camera plots to landscapes. *Remote Sens. Environ.* **177**, 13–20 (2016).
12. Lindenmayer, D., Franklin, J. & Fischer, J. General management principles and a checklist of strategies to guide forest biodiversity conservation. *Biol. Conserv.* **131**, 433–445 (2006).
13. De Frenne, P. & Verheyen, K. Weather stations lack forest data. *Science* **351**, 234–234 (2016).
14. Hoover, M. W. Some effects of temperature on the growth of southern peas. *Proc. Am. Soc. Hortic. Sci. USA* **66**, 308–312 (1955).
15. Reáumur, R. A. F. Observations du thermomètre, faites à Paris pendant l'année 1735, comparées avec celles qui ont été faites sous la ligne, à l'Isle de France, à Alger et en quelques-unes de nos isles de l'Amérique. *Mem. Acad. Sci. Paris* 545–576 (1735).
16. Cesaraccio, C., Spano, D., Duce, P. & Snyder, R. L. An improved model for determining degree-day values from daily temperature data. *Int. J. Biometeorol.* **45**, 161–169 (2001).
17. Miller, P., Lanier, W. & Brandt, S. *Using Growing Degree Days to Predict Plant Stages* (Montana State Univ., 2001).
18. Snyder, R. L., Spano, D., Cesaraccio, C. & Duce, P. Determining degree-day thresholds from field observations. *Int. J. Biometeorol.* **42**, 177–182 (1999).
19. Hamer, D. & Herrero, S. Grizzly bear food and habitat in the front ranges of Banff National Park, Alberta. *Bears Biol. Manag.* **7**, 199–213 (1987).
20. Laskin, D. N. & McDermid, G. J. Evaluating the level of agreement between human and time-lapse camera observations of understory plant phenology at multiple scales. *Ecol. Inform.* **33**, 1–9 (2016).
21. Misra, G., Buras, A. & Menzel, A. Effects of different methods on the comparison between land surface and ground phenology—a methodological case study from south-western Germany. *Remote Sens.* **8**, 753 (2016).
22. Yang, S. S., Logan, J. & Coffey, D. L. Mathematical formulas for calculating the base temperature for growing degree-days. *Agric. For. Meteorol.* **74**, 61–74 (1995).
23. Neteler, M., Roiz, D., Rocchini, D., Castellani, C. & Rizzoli, A. Terra and Aqua satellites track tiger mosquito invasion: modelling the potential distribution of *Aedes albopictus* in north-eastern Italy. *Int. J. Health Geogr.* **10**, 49 (2011).
24. Sun, Y. J. et al. Air temperature retrieval from remote sensing data based on thermodynamics. *Theor. Appl. Climatol.* **80**, 37–48 (2005).
25. Niclos, R., Valiente, J. A., Barbera, M. J. & Caselles, V. Land surface air temperature retrieval from EOS-MODIS images. *IEEE Geosci. Remote Sens. Lett.* **11**, 1380–1384 (2014).
26. De Frenne, P. et al. Microclimate moderates plant responses to macroclimate warming. *Proc. Natl Acad. Sci. USA* **110**, 18561–18565 (2013).
27. Laskin, D. N., Montaghi, A., Nielsen, S. E. & McDermid, G. J. Estimating understory temperatures using MODIS LST in mixed cordilleran forests. *Remote Sens.* **8**, 658 (2016).
28. Jang, K., Kang, S., Kimball, J. S. & Hong, S. Y. Retrievals of all-weather daily air temperature using MODIS and AMSR-E data. *Remote Sens.* **6**, 8387–8404 (2014).
29. Coops, N. C., Duro, D. C., Wulder, M. A. & Han, T. Estimating afternoon MODIS land surface temperatures (LST) based on morning MODIS overpass, location and elevation information. *Int. J. Remote Sens.* **28**, 2391–2396 (2007).
30. Crimmins, M. A. & Crimmins, T. M. Monitoring plant phenology using digital repeat photography. *Environ. Manage.* **41**, 949–958 (2008).
31. Huang, R. et al. Mapping of daily mean air temperature in agricultural regions using daytime and nighttime land surface temperatures derived from TERRA and AQUA MODIS data. *Remote Sens.* **7**, 8728–8756 (2015).
32. Laskin, D. N. Montaghi, A. & McDermid, G. J. An open-source method of constructing cloud-free composites of forest understory temperature using MODIS. *Remote Sens. Lett.* **8**, 165–174 (2017).
33. Metz, M., Rocchini, D. & Neteler, M. Surface temperatures at the continental scale: tracking changes with remote sensing at unprecedented detail. *Remote Sens.* **6**, 3822–3840 (2014).
34. Thomson, A. M. et al. RCP4.5: a pathway for stabilization of radiative forcing by 2100. *Climatic Change* **109**, 77 (2011).
35. Elith, J. & Leathwick, J. R. Species distribution models: ecological explanation and prediction across space and time. *Annu. Rev. Ecol. Evol. Syst.* **40**, 677–697 (2009).
36. Parmesan, C. Influences of species, latitudes and methodologies on estimates of phenological response to global warming. *Glob. Change Biol.* **13**, 1860–1872 (2007).
37. Crimmins, T. M., Crimmins, M. A., Gerst, K. L., Rosemartin, A. H. & Weltzin, J. F. USA National Phenology Network's volunteer-contributed observations yield predictive models of phenological transitions. *PLoS ONE* **12**, e0182919 (2017).
38. Melaas, E. K., Friedl, M. A. & Richardson, A. D. Multiscale modeling of spring phenology across deciduous forests in the eastern United States. *Glob. Change Biol.* **22**, 792–805 (2016).
39. Izquierdo-Verdiguier, E., Zurita-Milla, R., Ault, T. R. & Schwartz, M. D. Development and analysis of spring plant phenology products: 36 years of 1-km grids over the conterminous US. *Agric. For. Meteorol.* **262**, 34–41 (2018).
40. Primack, R. B. & Miller-Rushing, A. J. Broadening the study of phenology and climate change. *New Phytol.* **191**, 307–309 (2011).
41. Yu, R., Schwartz, M. D., Donnelly, A. & Liang, L. An observation-based progression modeling approach to spring and autumn deciduous tree phenology. *Int. J. Biometeorol.* **60**, 335–349 (2016).
42. Keenan, T. F. & Richardson, A. D. The timing of autumn senescence is affected by the timing of spring phenology: implications for predictive models. *Glob. Change Biol.* **21**, 2634–2641 (2015).
43. Liang, L., Schwartz, M. D. & Fei, S. Photographic assessment of temperate forest understory phenology in relation to springtime meteorological drivers. *Int. J. Biometeorol.* **56**, 343–355 (2012).
44. Zhang, F., Zhang, L. W., Shi, J. J. & Huang, J. F. Soil moisture monitoring based on land surface temperature-vegetation index space derived from MODIS data. *Pedosphere* **24**, 450–460 (2014).
45. Mendelsohn, R. et al. The ecosystem impacts of severe warming. *Am. Econ. Rev.* **106**, 612–614 (2016).
46. Stenset, N. E. et al. Seasonal and annual variation in the diet of brown bears *Ursus arctos* in the boreal forest of southcentral Sweden. *Wildlife Biol.* **22**, 107–116 (2016).
47. Deacy, W. W. et al. Phenological synchronization disrupts trophic interactions between Kodiak brown bears and salmon. *Proc. Natl Acad. Sci. USA* **114**, 10432–10437 (2017).
48. Kug, J.-S. et al. Two distinct influences of Arctic warming on cold winters over North America and East Asia. *Nat. Geosci.* **8**, 759–762 (2015).
49. Harsch, M. A. et al. Moving forward: insights and applications of moving-habitat models for climate change ecology. *J. Ecol.* **105**, 1169–1181 (2017).
50. Wan, Z. New refinements and validation of the collection-6 MODIS land-surface temperature/emissivity product. *Remote Sens. Environ.* **140**, 36–45 (2014).

Acknowledgements

The authors thank Alberta Innovates Biosolutions, the many partners of the Foothills Research Institute Grizzly Bear programme and programme lead G. Stenhouse for their generous funding and logistical support. Further thanks go to J. Woosaree, J. Newman and the staff at InnoTech Alberta for facilitating the growth-chamber experiments; R. Snyder for input on deriving base temperatures; and the NASA LP DAAC for access to the MODIS LST products. Additional funding support was provided by the Natural Sciences and Engineering Research Council of Canada (NSERC) through a Discovery Grant to G.J.M., Alberta Innovates, the University of Calgary and the Vanier Canada Graduate Scholarships Programme.

Author contributions

D.N.L., G.J.M., S.E.N. and S.J.M. conceived the study design. G.J.M., S.E.N. and S.J.M. supervised the analysis. D.N.L performed the data collection and experiments. S.E.N. and D.N.L developed the statistical analysis. D.R.R. produced the SDMs and downscaled the RCP4.5 anomaly surface. A.M. wrote the code for automating the MODIS LST image processing and analysis and D.N.L. wrote the manuscript. All authors contributed to manuscript editing.

Competing interests

The authors declare no competing interests.

Additional information

Supplementary information is available for this paper at https://doi.org/10.1038/s41558-019-0454-4.

Reprints and permissions information is available at www.nature.com/reprints.

Correspondence and requests for materials should be addressed to D.N.L.

Journal peer review information: *Nature Climate Change* thanks Eric Post and the other anonymous reviewer(s) for their contribution to the peer review of this work.

Methods

Overview. The phenology mapping framework comprises several methodological components which are described in detail in the following subsections (Supplementary Fig. 1). The first component encompasses the understory air-temperature modelling that bridges the gap between canopy-top observations of MODIS LST and underlying air temperatures (T_{ust}). The next component works to produce the present-day phenology maps by extending the plot-scale T_{ust} estimates across the landscape. The resulting landscape-scale T_{ust} image stack is transformed into daily phenology maps by summing the seasonal thermal accumulation (AGDD) of each image pixel. AGDD is the thermal energy required to physiologically transition from one phenophase to the next. The final methodological component forecasts the 2080s phenology by modifying the present-day phenology maps using a downscaled regional RCP4.5 anomaly estimated from a multi-model ensemble from the fifth phase of the Coupled Model Intercomparison Project (CMIP5)[51]. In essence, the anomaly is integrated into the present-day T_{ust} maps to project the effects of climate change onto existing patterns of understory phenology. This modelled forecast was contrasted with experimental warming of *S. canadensis* to determine a calculable phenological response of the target species to an end-of-century scenario.

In situ phenology and temperature observations. A digital camera network of 85 Wingscapes PlantCams was distributed in 45 forested plots throughout the study area over two seasons in 2011 and 2012. Within each plot, at least one plant was identified and imaged daily at solar noon by one or two cameras. *S. canadensis* was selected as the focal species because of its widespread distribution, visually distinct phenophases and critical nutritional importance for vertebrates, including threatened populations of grizzly bears. Observations were made of the structural–physical reproductive phenology and they were assigned a discrete designation based on the current stage of development. The phenophases were based on those developed by Dierschke[52], but were modified to better suit the purposes of this framework. Sub-canopy air temperature accumulations were recorded at hourly intervals (error no greater than ±0.5 °C) using Thermochron temperature loggers (Maxim Integrated Products) placed within solar radiation shields 1 m above ground, the approximate height of shrubby vegetation. Twenty-nine of the 45 plots were 250 m × 250 m (6.25 ha) in size to approximate the resolution of the thermal satellite imagery[21]. These plots were located within large homogeneous forest stands with four additional gridded sensors to record average T_{ust} within the stand. Field visits were made by personnel at intervals <10 d to corroborate the camera imagery and to make phenological observations of the surrounding 6.25 ha plots along two stratified random 250 m sample transects. We used error matrices[53] to evaluate the level of agreement between the photo- and field-derived phenophases. The reference observations were those identified by personnel in the field, to which the camera images were then matched by date. A weighted kappa statistic[54] was calculated to evaluate the strength of agreement between the two methods of observation[20]. There was no significant difference between phenophases observed from a solitary camera–plant pairing and the other *S. canadensis* plants throughout the broader study plot ($z = 0.042$, $P = 0.996$). This result suggests that there may be little benefit in observing more than a single plant to approximate the phenology of a region up to 6.25 ha or potentially larger. The broader spatial extent of these plots corresponds with the areal unit scale of the satellite image pixels, and was the initial step in coupling the phenology of individual plants to the broader landscape.

Estimating understory temperature from MODIS LST. Generalized linear models (GLMs) were derived in STATA 13 statistical software[55] to estimate instantaneous values of T_{ust} at the plot scale. Random effects were used to offset bias from repeated temperature observations within single sites, and candidate-model selection was performed using Akaike's information criterion. The daily 1 km LST product is collected by NASA's EOS sun-synchronous, near-polar orbiting Terra and Aqua satellites. With Aqua in an ascending orbit and Terra in a descending orbit, the two platforms deliver a total of four daily equatorial crossings at 13:30, 01:30, 10:30 and 22:30 (local solar time)[56]. We used the following two LST image products: Terra MOD11A1 and Aqua MYD11A1. In addition to MODIS LST, Julian day (quadratic polynomial) was used to express growing-season duration[29,57]. Environmental lapse rate varies substantially with altitude, so elevation was added as a covariate derived from a 10 m photogrammetrically compiled digital elevation model[58]. Forest and overstory covariates included canopy closure (%), forest-stand type (characterized as the proportion of conifer trees) and a suite of LiDAR-derived canopy metrics. Canopy closure and the proportion of conifer were measured in situ every 50 m (14 sub-plots) along two 250 m stratified-random linear transects in the 6.25 ha plots. Canopy closure was measured during leaf-on conditions using five vertical hemispherical photographs at each sub-plot and later processed with WinSCANOPY software[59]. A representative sample of tree species was obtained using a 360° sweep of each sub-plot using a wedge prism relascope. Laskin et al.[32] developed a procedure to extend the instantaneous estimates of plot-scale T_{ust} into spatially continuous, cloud-free maps of daily average T_{ust} at the landscape scale. GLMs were again used to estimate daily average T_{ust} from each of the four daily MODIS overpasses (to within 1.5 °C, $R^2 \approx 0.87$), first at the plot scale to acquire the model coefficients and then extending these models across the 125,000 km² study area. All of the model covariates were previously modelled at 30 m Landsat resolution using nearly 1,000 ground-truth locations[60], enabling the translation of the models to wall-to-wall estimates of daily average T_{ust}. During this step, the estimates of T_{ust} were spatially enhanced to 250 m using the higher-resolution covariate rasters (that is, elevation) to augment the 1 km LST data[61] and match the areal-unit scale of the in situ measurements. The four daily estimations of average T_{ust} at 250-m resolution were then stacked and merged into a single daily image to increase the cloud-free coverage, averaging T_{ust} values wherever there was any overlap[31]. The remaining cloud gaps were filled with Gaussian-weighted temporal interpolation using clear-sky values from ±7 d preceding and following the current image date[33,62]. A cloudiness coefficient was used to offset the bias of estimating higher temperatures within cloud gaps resulting from the use of temporally adjacent clear-sky (warmer) pixels. The final daily T_{ust} averages were compared to randomly selected daily in situ averages during all weather conditions (20% proportion of the training data). The T_{ust} models were also compared against air temperature (T_{air}) estimates in a non-forested validation plot (6.25 ha) by recording in situ air temperature over two seasons at the centre of a broad expanse (2,700 km²) of native grassland, which provided near-perfect homogeneous land cover. We used an identical sample design to train the null model for solely LST and date. Air temperature estimates in the validation plot had an average root-mean-square error increase of 2 °C compared with the forest plots. This result supports the notion that estimates of T_{air} using LST are generally more accurate over forest cover[63], while also demonstrating the efficacy of the framework beyond forests.

GDDs and developmental-threshold temperatures. There are a variety of techniques for calculating GDDs[64,65], but the principal form of the equation is as follows[66]:

$$\mathrm{GDD} = \left[\frac{T_{max} + T_{min}}{2}\right] - t_b \quad (1)$$

where T_{max} and T_{min} are the temperature extremes reached in a single 24-h period, and t_b is the base temperature, or minimum physiological temperature threshold. For this study, threshold temperatures were derived using a statistical approach recommended by Yang et al.[22] called the regression method, originally developed by Hoover[14]. A statistical-threshold temperature is derived by minimizing the standard deviation in AGDD between phenophases over a series of observations. The regression method was used to obtain the developmental threshold using observations from across the study area and within the growth chambers. The methodology used by Yang et al.[22], as described by Snyder et al.[18], begins by defining one season of phenological observations of a single plant as a case, and the total GDD, or $[f_i(t_b)]$, as a function of the threshold temperature (t_b) for the ith case as:

$$f_i(t_b) = (T_i - t_b)\, d_i \quad (2)$$

here, T_i is the sum of the daily mean temperatures divided by the number of days in the ith case (d_i), and t_b is the base threshold temperature. The resulting GDD values are plotted against the daily mean temperatures during the corresponding phenophases. The threshold value is found by iterating until the slope of the regression equals zero and solving for t_b:

$$t_b = \frac{\sum T_i \sum d_i T_i - n \sum d_i T_i^2}{\sum d_i \sum T_i - n \sum d_i T_i} \quad (3)$$

The reproductive temperature threshold for *S. canadensis* was calculated to be 0 °C ± 0.6 °C in both the field and growth-chamber case observations. The GDD accumulations were then quantified for each discrete phenophase start date in the seasonal progression.

Present-day phenology maps. The baseline year 2012 was selected to characterize phenological timing within the study area and represents the present-day climate scenario. Of the two years of field observations, 2012 was the closest in temperature to the 30-year study-area average (February-to-October average to within 0.33 °C). This was confirmed using gridded monthly temperature from the National Oceanographic and Atmospheric Administration (NOAA) North American Regional Reanalysis dataset (NARR). Daily average T_{ust} maps were produced from the beginning of February, well before any location reached average temperatures above freezing, until the end of October. The production of the phenology maps was semi-automated using scripts developed in the statistical programming language R[67] and the Python 2.7 environment[68]. The GDD equation (equation (1)) was applied to each T_{ust} image in the raster stack, producing an output of the daily accumulations above the threshold temperature. The imagery was then classified on the basis of the AGDD required to begin each phenophase. The final product was a time series of the complete phenological progression of *S. canadensis* across the study area. The AGDD requirements were calculated from field observations from 2011 and validated using independent observations made at 16 new plots in 2012. The maps were validated by calculating the MAE between the map-predicted start date of each phenophase and the actual start date observed at each individual plant on the ground (plot scale). A paired t-test was used to determine whether

there was a significant difference between the map predictions and observed in situ phenophases.

Future phenology maps. Future phenology projections were based on the RCP4.5 scenario of IPCC AR5 for the 2080s decadal average[69]. Rather than selecting a single general circulation model (GCM) projection, which could produce bias, we used an ensemble average of 15 individual GCM projections from the CMIP5: CSIRO-ACCESS1.0, CCCMA-CanESM2, NCAR-CCSM4, NCAR-CESM1-CAM5, CNRM-CM5, CSIRO-Mk3-6-0, GFDL-CM3, GISS-E2R, HadGEM2-ES, INM-CM4, IPSL-CM5S-MR, MIROC5, MIROC-ESM-LR, MPI-ESM-LR and MRI-CGCM3. The ensemble output was averaged and downscaled to a 1-km resolution anomaly surface for the study area ranging between +3.1 °C and +3.4 °C (mean: +3.29 °C) using ClimateNA v.5.4[70]. These values were added to each of the daily average T_{ust} time-series images in the stack to create a corresponding daily future temperature scenario within the study area. The AGDD were recalculated using the same developmental base temperature ($t_b = 0$ °C), and reclassified using the same GDD requirements.

Species-distribution models. Species-distribution models (SDMs) were used both to characterize present-day habitat of *S. canadensis* (1961–1990) and to project the species' range under future climate change scenario RCP4.5 (2080s). The SDMs were used to spatially mask the corresponding phenology maps. SDM development followed the methodology outlined in Roberts et al.[71], with some data and methodology updates. Models were trained on 7,088 species-survey plots with covariates that included present-day and future climate data obtained from ClimateNA v.5.4 (including the RCP4.5 GCM ensemble described above) and a selection of ten biologically relevant annual and seasonal climate variables (assessed for collinearity): mean annual temperature (°C), average summer temperature (°C), average winter temperature (°C), extreme minimum temperature (°C), total summer precipitation (mm), total winter precipitation (mm), Hargreave's annual climate moisture deficit (mm), Hargreave's summer climate moisture deficit (mm), number of degree days above 5 °C (days) and number of frost-free days (days). For our variable definitions, summer is defined as the months of June, July and August, and winter is defined as the months of December, January and February. We also included three topo-edaphic variables as predictors: compound topographic index (unitless), topographic heat-load index (unitless), and topographic radiation aspect (unitless). Last, we included a remotely sensed measure of forest-crown closure (%). Whereas most topo-edaphic variables remain constant over time, crown closure may change with changing climates. To achieve values for the future we projected crown closure using a random forest-modelling approach, trained with remotely sensed crown-closure values and all 13 climate and topo-edaphic variables listed above. We then projected crown-closure values for the 1961–1990 normal period as well as for the 2080s using the same RCP4.5 ensemble GCM projection used in the SDM. We employed an ensemble SDM approach using the biomod2 package for R[72] to create several SDMs using eight individual approaches trained on 7,088 modern species-survey plots: GLMs, generalized additive models (GAMs), generalized boosted models (GBMs), classification tree analysis (CTA), artificial neural networks (ANN), multivariate adaptive regression splines (MARS), random forest (RF) and Phillips' maximum entropy (MAXENT). From these individual models, a single ensemble projection was created by averaging the individual model outputs. The ensemble models generated probability-of-presence (between 0 and 1) values across the study area at a resolution of 300 m × 300 m. Probability-of-presence surfaces were subsequently converted to binary maps of *S. canadensis* presence and absence using a conservative receiver-operating characteristic (area under curve, AUC) threshold of 3.25. Ensemble SDM projections (mean projections of individual SDM approaches) were evaluated using the AUC via two *k*-fold cross-validations. The first incorporated 17 random data splits (that is, 17 folds), whereas the second incorporated spatially blocked data splits of approximately 100 km × 100 km each. Incorporating spatial blocks into cross-validations addresses residual autocorrelation as well as potential model overfit to underlying data structures, both of which can result in overly optimistic validations[73]. AUC for the random and blocked cross-validations were 0.82 and 0.78, respectively. In the future models, it is assumed that *S. canadensis* is not in a state of transition or adaptation to novel climatic environments and that observed patterns reflect the species' full biotic potential by occupying all environmentally suitable areas[74].

Growth-chamber observations. We used experimental warming to observe shifts in the timing of reproductive phenology in *S. canadensis*[75–78]. Considering that climate change affects taxa in different ways[7], we directly tested the sensitivity of *S. canadensis* to warming to evaluate the projected advances observed in the future phenology maps. Experiments were conducted at an agricultural research facility (Innotech Alberta) using eight fully enclosed Conviron E15 climate-controlled growth chambers with light intensity and photoperiod control and refrigeration to simulate night and early-season conditions. Two scenarios were reproduced in the chambers: a present-day control (2012) and the end-of-century RCP4.5 scenario (2080s). The present-day temperature profile was established on a 30-year average at an Environment Canada weather station located near the centre of the study area (53° 14′ N, 117° 49′ W). The future warming profile was based on the downscaled regional RCP4.5 anomaly with a mean of +3.3 °C. AR5 projections for western Canada are much higher than the global average, with a maximum difference of +4 °C (ref. [79]). Two eight-month observation 'seasons' were enacted using 20 adult plants in 2013 and 26 in 2014, proportionately divided and assigned randomly into present-day control and RCP4.5 scenario chambers. Each plant was monitored daily by a PlantCam and additional intermittent DSLR imagery. Four visually distinct phenophases were selected for observation to maximize temporal precision and bookend the critical reproductive phenology of this species: first flower, full bloom, first ripe and fully ripe. The developmental variance between chambers was calculated as the mean difference in days for each of these phenophases. To ensure fruit production, male plants in each chamber were used to hand-pollinate flowers in lieu of insects. Pollination took place whenever a plant attained full bloom (>90% of flowers visible) in both the control and treatment chambers to limit temporal bias in the subsequent phenophases. All plants were simultaneously cold-stratified for five months preceding chamber observations at a constant temperature of −5 °C to simulate winter. Lighting intensity was calibrated and kept constant within the chambers with diurnal and seasonal photoperiod corresponding to mid-latitude of the study area[80]. Moisture levels and watering schedules were also kept as consistent as possible. There were no adjustments made for RCP4.5 precipitation forecasts since end-of-century projections are mixed for southwestern Alberta with no statistically significant trend in the composite models[79].

Data availability

Daily MODIS LST imagery products are available from the NASA Land Processes Distributed Active Archive Center (LP DAAC, http://lpdaac.usgs.gov). The data that support the findings of this study are available from the corresponding author on reasonable request.

Code availability

The computer code and algorithms generated during this study are available from the corresponding author on reasonable request.

References

51. Taylor, K. E., Stouffer, R. J. & Meehl, G. A. An overview of CMIP5 and the experiment design. *Bull. Am. Meteorol. Soc.* **93**, 485–498 (2012).
52. Dierschke, H. On the recording and presentation of phenological phenomena in plant communities (trans. Wessell, R. E. & Talbot, S. S.). In *International Symposium for Vegetation Science* (IVV, 1972).
53. Congalton, R. G. & Green, K. *Assessing the Accuracy of Remotely Sensed Data: Principles and Practices* (CRC, 2002).
54. Altman, D. G. *Practical Statistics for Medical Research* (CRC, 1991).
55. Stata v.13.0 (Stata Corporation, 2013).
56. Williamson, S. N., Hik, D. S., Gamon, J. A., Kavanaugh, J. L. & Koh, S. Evaluating cloud contamination in clear-sky MODIS TERRA daytime land surface temperatures using ground-based meteorology station observations. *J. Clim.* **26**, 1551–1560 (2013).
57. Benali, A., Carvalho, A. C., Nunes, J. P., Carvalhais, N. & Santos, A. Estimating air surface temperature in Portugal using MODIS LST data. *Remote Sens. Environ.* **124**, 108–121 (2012).
58. Rhee, J. & Im, J. Estimating high spatial resolution air temperature for regions with limited in situ data using MODIS products. *Remote Sens.* **6**, 7360–7378 (2014).
59. Winscanopy v.2006c (Regent Instruments, 2006).
60. Linke, J. et al. The influence of patch-delineation mismatches on multi-temporal landscape pattern analysis. *Landscape Ecol.* **24**, 157–170 (2009).
61. Zorer, R. et al. Daily MODIS land surface temperature data for the analysis of the heat requirements of grapevine varieties. *IEEE Trans. Geosci. Remote Sens.* **51**, 2128–2135 (2013).
62. Neteler, M. Estimating daily land surface temperatures in mountainous environments by reconstructed MODIS LST data. *Remote Sens.* **2**, 333–351 (2010).
63. Mostovoy, G. V., King, R. L., Reddy, K. R., Kakani, V. G. & Filippova, M. G. Statistical estimation of daily maximum and minimum air temperatures from MODIS LST data over the state of Mississippi. *GISci. Remote Sens.* **43**, 78–110 (2006).
64. Snyder, R. L. Hand calculating degree days. *Agric. For. Meteorol.* **35**, 353–358 (1985).
65. Roltsch, W. J., Zalom, F. G., Strawn, A. J., Strand, J. F. & Pitcairn, M. J. Evaluation of several degree-day estimation methods in California climates. *Int. J. Biometeorol.* **42**, 169–176 (1999).
66. McMaster, G. S. & Wilhelm, W. W. Growing degree-days: one equation, two interpretations. *Agric. For. Meteorol.* **87**, 291–300 (1997).
67. R Development Core Team *R: A Language and Environment for Statistical Computing* (R Foundation for Statistical Computing, 2018).
68. Python Language Reference v.2.7.0 (PythonLabs, 2010).
69. IPCC *Climate Change 2014: Synthesis Report* (eds Core Writing Team, Pachauri, R. K. & Meyer L. A.) (IPCC, 2014).

70. Wang, T., Hamann, A., Spittlehouse, D. & Carroll, C. Locally downscaled and spatially customizable climate data for historical and future periods for North America. *PLoS ONE* **11**, e0156720 (2016).
71. Roberts, D. R., Nielsen, S. E. & Stenhouse, G. B. Idiosyncratic responses of grizzly bear habitat to climate change based on projected food resource changes. *Ecol. Appl.* **24**, 1144–1154 (2014).
72. Thuiller, W., Lafourcade, B., Engler, R. & Araújo, M. B. BIOMOD—a platform for ensemble forecasting of species distributions. *Ecography* **32**, 369–373 (2009).
73. Roberts, D. R. et al. Cross-validation strategies for data with temporal, spatial, hierarchical, or phylogenetic structure. *Ecography* **40**, 913–929 (2017).
74. Barry, S. & Elith, J. Error and uncertainty in habitat models. *J. Appl. Ecol.* **43**, 413–423 (2006).
75. Norby, R. J., Hartz-Rubin, J. S. & Verbrugge, M. J. Phenological responses in maple to experimental atmospheric warming and CO_2 enrichment. *Glob. Change Biol.* **9**, 1792–1801 (2003).
76. Sherry, R. A. et al. Divergence of reproductive phenology under climate warming. *Proc. Natl Acad. Sci. USA* **104**, 198–202 (2007).
77. Clark, J. S., Salk, C., Melillo, J. & Mohan, J. Tree phenology responses to winter chilling, spring warming, at north and south range limits. *Func. Ecol.* **28**, 1344–1355 (2014).
78. Kopp, C. W. & Cleland, E. E. A. A range-expanding shrub species alters plant phenological response to experimental warming. *PLoS ONE* **10**, 0139029 (2015).
79. van Oldenborgh, G. J. et al. in *Climate Change 2013: The Physical Science Basis* (eds Stocker, T. F. et al.) Annex 1 (IPCC, Cambridge Univ. Press, 2013).
80. Way, D. A. & Montgomery, R. A. Photoperiod constraints on tree phenology, performance and migration in a warming world. *Plant Cell Environ.* **38**, 1725–1736 (2015).